Article

Ebola Virus VP24 Targets a Unique NLS Binding Site on Karyopherin Alpha 5 to Selectively Compete with Nuclear Import of Phosphorylated STAT1

Wei Xu,[1] Megan R. Edwards,[2] Dominika M. Borek,[3] Alicia R. Feagins,[2] Anuradha Mittal,[4] Joshua B. Alinger,[1] Kayla N. Berry,[1] Benjamin Yen,[2] Jennifer Hamilton,[2] Tom J. Brett,[5] Rohit V. Pappu,[4] Daisy W. Leung,[1] Christopher F. Basler,[2] and Gaya K. Amarasinghe[1],*

[1]Department of Pathology and Immunology, Washington University School of Medicine, St Louis, MO 63110, USA
[2]Department of Microbiology, Icahn School of Medicine at Mount Sinai, New York, NY 10029, USA
[3]Departments of Biophysics and Biochemistry, University of Texas Southwestern Medical Center at Dallas, Dallas, TX 75390, USA
[4]Department of Biomedical Engineering and Center for Biological Systems Engineering, Washington University, St. Louis, MO 63110, USA
[5]Department of Internal Medicine, Washington University School of Medicine, St. Louis, MO 63110, USA
*Correspondence: gamarasinghe@path.wustl.edu
http://dx.doi.org/10.1016/j.chom.2014.07.008

SUMMARY

During antiviral defense, interferon (IFN) signaling triggers nuclear transport of tyrosine-phosphorylated STAT1 (PY-STAT1), which occurs via a subset of karyopherin alpha (KPNA) nuclear transporters. Many viruses, including Ebola virus, actively antagonize STAT1 signaling to counteract the antiviral effects of IFN. Ebola virus VP24 protein (eVP24) binds KPNA to inhibit PY-STAT1 nuclear transport and render cells refractory to IFNs. We describe the structure of human KPNA5 C terminus in complex with eVP24. In the complex, eVP24 recognizes a unique nonclassical nuclear localization signal (NLS) binding site on KPNA5 that is necessary for efficient PY-STAT1 nuclear transport. eVP24 binds KPNA5 with very high affinity to effectively compete with and inhibit PY-STAT1 nuclear transport. In contrast, eVP24 binding does not affect the transport of classical NLS cargo. Thus, eVP24 counters cell-intrinsic innate immunity by selectively targeting PY-STAT1 nuclear import while leaving the transport of other cargo that may be required for viral replication unaffected.

INTRODUCTION

Interferons (IFNs) generate innate and adaptive immune responses to viral infections through a signaling cascade that requires the activation of signal transducer and activator of transcription (STAT) family transcription factors (Goodbourn et al., 2000). Type I IFNs activate STAT1 and STAT2 through phosphorylation by the Janus kinase (JAK) family members, and type II IFN only activates STAT1 (Reich and Liu, 2006). Phosphorylation of tyrosine 701 on STAT1 (PY-STAT1) results in a conformation that is recognized by a subset of the karyopherin alpha (KPNA) family of nuclear transport factors (Chen et al.,

1998; McBride et al., 2002; Meyer et al., 2002). Nuclear transport of PY-STAT1 and binding to IFN-stimulated response elements (ISRE) or interferon-gamma-activated site (GAS) elements induce expression of IFN-stimulated genes (ISG) that confer an antiviral state.

All KPNAs contain ten armadillo (ARM) repeats and are divided into subfamilies based on sequences that dictate cargo specificity (Conti and Kuriyan, 2000; Conti et al., 1998). Cargo that contain a classical nuclear localization signal (cNLS), which consists of mostly basic amino acids, bind KPNA near ARMs 2–4 (major site) and 6–8 (minor site) (Chook and Blobel, 2001; Conti and Izaurralde, 2001; Cook et al., 2007). In contrast, the NPI-1 subfamily (KPNA1, KPNA5, and KPNA6; also known as importin α5, importin α6, and importin α7, respectively) mediates PY-STAT1 nuclear transport, which depends on a nonclassical NLS (ncNLS) (Sekimoto et al., 1997). Use of a distinct nuclear transporter binding site presumably allows PY-STAT1 to translocate to the nucleus without impacting regular nucleocytoplasmic trafficking processes. Viruses target IFN signaling by inhibiting distinct steps in the STAT1 activation and nuclear translocation process, but these mechanisms vary, and many are poorly defined (Yarbrough et al., 2014).

A hallmark of infection by filoviruses (Ebola virus [EBOV] and Marburg virus [MARV]) is the rapid and potent suppression of innate antiviral immune responses, which facilitates uncontrolled viral replication and cytokine storm (Bray and Murphy, 2007; Geisbert et al., 2003). As a result, high case fatality rates of up to 90% are observed during outbreaks (Feldmann and Geisbert, 2011). EBOV mediates immune suppression through at least three virally encoded proteins: surface glycoprotein (GP), virus protein 35 (eVP35), and virus protein 24 (eVP24) (Basler and Amarasinghe, 2009; Kaletsky et al., 2009; Leung et al., 2010; Zhang et al., 2012a). Among these, eVP24 acts in a cell-intrinsic manner to inhibit IFN signaling and render cells refractory to exogenous IFN treatment by targeting the NPI-1 subfamily of KPNAs, but the molecular mechanism of this process is unknown.

Cargo containing ncNLS sequences are often difficult to identify because ncNLS sequences lack consensus motifs. As a result, the exact ncNLS binding site for PY-STAT1 as well as viral
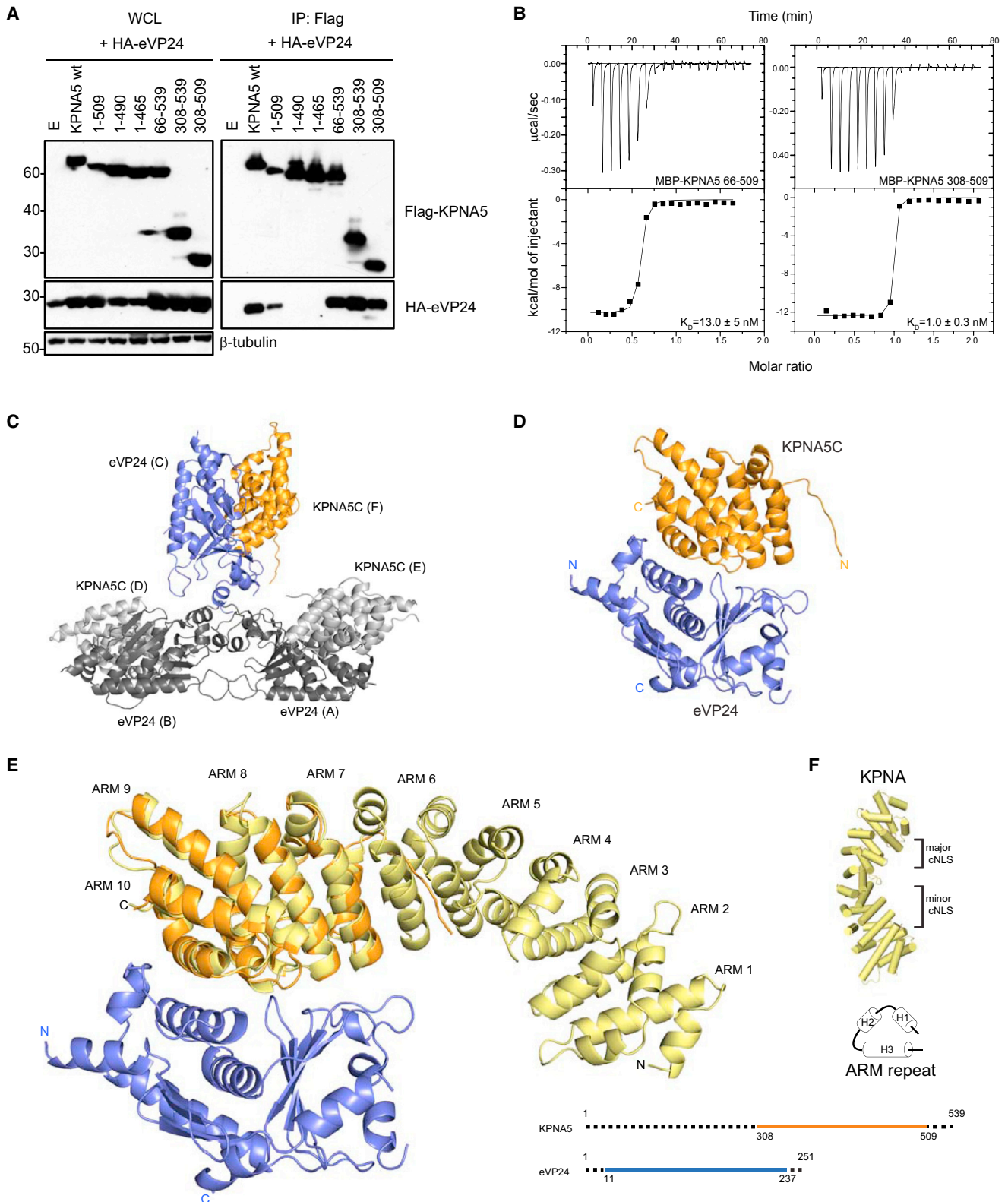
Figure 1. eVP24 Binds an ncNLS Site on KPNA5 Near C-Terminal ARMs 8, 9, and 10 with High Affinity and Specificity

(A) Coimmunoprecipitation experiments with FLAG antibody were performed from lysates of 293T cells cotransfected with plasmids for Flag-KPNA5 of various lengths, as indicated in the figure and HA-eVP24. Western blots were performed for FLAG, hemagglutinin (HA), and β-tubulin. WCL, whole-cell lysate.

Table 1. Data Collection, Structure Solution Statistics, and Validation Results

Data Collection	
Space group	$P3_121$
Unit Cell Parameters	
a, b, c (Å)	103.93, 103.93, 333.63
α, β, γ (°)	90, 90, 120
Resolution range (Å)	50–3.15 (3.20–3.15)*
Unique reflections	35,719 (1735)
Redundancy	6.0 (6.0)
Completeness (%)	96.2 (98.1)
R_{merge} (%)	9.1 (95.3)
$<I> / <\sigma\ (I)>$	14.8 (1.1)
CC1/2	(0.546)
Structure Solution and Refinement	
Resolution (Å)	35.12–3.15 (3.23–3.15)
Number of reflections	29,294
Completeness (%)	83.2 (37.2)
Nonhydrogen atoms	9,199
R_{work}/R_{free} (%)	21.6/24.9 (27.5/29.7)
Rmsd	
Bond lengths (Å)	0.004
Bond angles (°)	0.824
B Factors (Å^2)	
Protein (chain A)	29.28
Protein (chain B)	29.42
Protein (chain C)	42.88
Protein (chain D)	53.52
Protein (chain E)	33.08
Protein (chain F)	52.91
Water	28.92
Ramachandran plot outliers (%)	0.26
MolProbity score	1.18
MolProbity clashscore	1.73

Summary of data collection and structure solution statistics for the eVP24 and KPNA5C complex and validation results from the MolProbity server. *Values in parentheses are for the highest-resolution shell.

antagonists that bind nuclear transporters has not been characterized. In order to address this limitation, we characterized the binding between eVP24 and the NPI-1 subfamily of karyopherins by truncation/mutational analysis and defined the minimal structured region of eVP24 and C terminus of KPNA5 (KPNA5C). Using these minimal protein constructs, we determined the crystal structure of the eVP24 and KPNA5C complex. With the structure as a guide, we characterized eVP24 and PY-STAT1 binding to the nuclear transporter as well as the mechanism of innate immune antagonism by eVP24. The data reveal direct competition between eVP24 and PY-STAT1 for the NPI-1 subfamily of nuclear transporters, which promotes inhibition of cell-intrinsic innate immune response and renders Ebola virus-infected cells insensitive to IFN treatment.

RESULTS

KPNA5 C Terminus Is Necessary and Sufficient for eVP24 Binding

In order to gain mechanistic insight into how eVP24 promotes immune suppression, we characterized the eVP24/KPNA5 interaction. We used a series of Flag-KPNA5 truncation mutants from which we identified residues 308–509 (KPNA5C) encompassing ARMs 7–10 as the minimal region necessary for binding to eVP24 (1–251) (Figure 1A). Next, we carried out quantitative isothermal titration calorimetry (ITC) studies, which revealed that KPNA5C and ΔIBB-KPNA5 (66–509; lacking the importin β binding region and the extreme C terminus) each bound eVP24 with similar high affinities (Figure 1B), suggesting that key binding determinants are located in KPNA5C. Using the minimal constructs, we determined the crystal structure of the KPNA5C and eVP24 complex to a 3.1 Å resolution in order to further define the molecular basis of the interaction interface. There are three copies of the complex in the asymmetric unit, each consisting of KPNA5C and eVP24 (Figures 1C–1D and Table 1). Structural comparison of eVP24 protein in the complex to the free form suggests limited structural change upon complex formation, as we observe only 0.83 Å backbone root-mean-square deviation (rmsd) between these two structures (Figure S1, available online). In comparison to previous KPNA structures, the KPNA5 ARMs 7–10 in the eVP24/KPNA5C complex also show only minor conformational changes upon eVP24 binding, and correspondingly the backbone rmsd for ARMS 7–10 is 0.98 Å (Figure 1E). Collectively, these results demonstrate that ARMs 7–10 are sufficient to bind eVP24; however, as discussed below, the minimal binding region for eVP24 on KPNA5 is likely contained within ARMs 8–10 based on analysis of the complex.

The eVP24/KPNA5C Complex Reveals a Unique ncNLS Binding Site

In the eVP24/KPNA5C structure, the interface between the two molecules buried about 2,100 Å^2 of solvent accessible surface area (Figure S2). In addition to burying a large solvent accessible surface area, this interface displays high shape complementarity judging from the shape complementary value Sc = 0.82 (for

(B) Raw ITC data and corresponding binding isotherms for MBP-tagged eVP24 (residues 11–237) binding to KPNA5 66–509 (left) and KPNA5C (right). Representative data are shown from at least two independent experiments. Control experiments show that MBP does not bind KPNA5 or KPNA5C.

(C) Asymmetric unit of eVP24/KPNA5C complex contains three complexes with 1:1 stoichiometry. eVP24 is shown in blue (mol C) and dark gray (mol A and B); KPNA5C is shown in orange (mol F) and light gray (mol D and E). Only eVP24 residues 16–231 and KPNA5C residues 332–506 were modeled in the final refined structure.

(D) Representative 1:1 complex structure between eVP24/KPNA5C reveals multiple structural interaction elements between the two molecules.

(E) Alignment of a KPNA structure (yellow; PDB ID: 1BK5) with the C-terminal ARM repeats from the eVP24/KPNA5C complex structure.

(F) The three-helix construction of the ARM repeats and the ten ARM repeats of KPNA proteins are shown. cNLS and ncNLS sites are marked. See also Figures S1 and S5.

reference, antibody/antigen complexes show Sc > 0.75). Analysis of residues in the interface reveals that the interface is largely hydrophobic. Moreover, only limited charge complementarity is observed (Figure S2B). eVP24 interacts with KPNA5 ARMs 8, 9, and 10 (Figures 1E and 1F), which is a unique ncNLS binding site for KPNA transporters (Cook et al., 2007; Yarbrough et al., 2014). In the structure of the complex, there are three clusters of eVP24 residues that contact KPNA5C (Figures 2, S1, and S3A). A majority of cluster 1 contacts are derived from helix 6 to helix 7, including the linker between helices 6 and 7. Contact residues include L115, L121, W125, T128, T129, N130, T131, N135, R137, T138, and R140 (Figure 2). In addition, there are interactions with KPNA5 ARMs 8–9 and 9–10 by eVP24 residues Q184, N185, and H186 (cluster 2) and D124, T128, and T129, respectively (Figure 2). The third cluster (cluster 3) of residues is between 201 and 207, including L201, E203, P204, D205, and S207, which show hydrogen bonds and nonbonded contacts with KPNA5. eVP24 helix 6 and the helix 2 from ARMs 9 and 10 of KPNA5C form a hydrophobic core, which appears to provide high shape complementarity and buries a large surface area at the interface. Amino acids 142–146 were defined previously as being important for KPNA5 binding (Mateo et al., 2010). Although these are not located in the binding interface, the proximity of residues 142–146 to contact residues suggests that their mutation may influence the conformation of contact residues (Mateo et al., 2010). Overall, the structure reveals that eVP24 contributes a large number of residues to the binding interface and that the sites of interaction on KPNA5 appear to be distinct from previously described binding sites for other KPNA interactors, including ncNLS-containing cargo (Cook et al., 2007; Yarbrough et al., 2014).

KPNA5 ARM10 Is Required for eVP24 Binding

eVP24 selectively targets PY-STAT1 binding to the NPI-1 subfamily of KPNAs and fails to interact with non-NPI-1 subfamily KPNAs 2, 3, and 4, which also do not recognize PY-STAT1 (Reid et al., 2007). The structure indicates that fewer KPNA5 residues than eVP24 residues contribute to the binding interface (23 for eVP24 versus 15 for KPNA5) (Figure 2). In all, we observe 15 conserved residues, of which 10 are identical in the NPI-1 subfamily (Figure S3B). Of these KPNA5 residues, some located in ARM10 helix 1 and helix 2, including E474, E475, D480, K481, and E483, contact eVP24 (Figure 2C) but are not required for eVP24 interactions, as mutation of these residues only shows slightly diminished binding (Figure 3). In contrast, interface residues R396, R398, D431, V435, M436, Y477, F484, and S487 are conserved only in the NPI-1 subfamily of KPNA1, KPNA5, and KPNA6, but not in the non-NPI-1 subfamily KPNA2, KPNA3, and KPNA4. These NPI-1-specific interface residues in the eVP24/KPNA5 complex may explain how eVP24 achieves specificity for the NPI-1 subfamily of KPNAs despite high sequence and structural similarities among KPNA proteins. Among the three clusters that contact KPNA5, clusters 1 and 3 are conserved among different EBOV but vary between eVP24 and MARV VP24 (mVP24), which, despite homology to eVP24, does not block IFN signaling (Figure S3A) (Valmas et al., 2010). This suggests that these two clusters may serve as the specificity determinants of eVP24. In addition to these sequence-based assessments, further structural analysis of eVP24 and

mVP24 also supports the importance of residues from clusters 1 and 3 as important contributors to KPNA binding.

In the structure, KPNA5 ARM 10 helix 3 appears to stabilize the structural features recognized by eVP24. Although ARM10 helix 3 does not contact eVP24 in the structure, it is still important for interaction, as deletion of helix 3 results in loss of binding (Figure 1A; 1–490 KPNA5). In the absence of evidence for direct contact, we can attribute a structural role for helix 3, where helix 3 may stabilize ARM10 helices 1 and 2, the two helices in ARM10 that contact eVP24. To address this possibility, we assessed the helical stability of ARM10 using atomistic simulations. The results show that helices 1 and 2 are highly unstable in isolation. However, the helicities of these segments increase significantly when they are in the context of ARMs 7–9 and helix 3 from ARM 10 (Figure 2D). These results demonstrate that KPNA5 ARM10 is a major binding determinant that also contributes to the binding specificity of eVP24.

eVP24 Makes Extensive Multiresidue Contacts at the Interface

We evaluated the contributions of individual amino acids of eVP24 to the KPNA5 binding interface by coimmunoprecipitation (coIP). A list of mutations used in the study is shown in Figures 3A and 3B. With the exception of R137A, all single eVP24 point mutants tested showed only minor (<20%) loss of KPNA5 binding (Figure 3C). In contrast, several multiresidue mutants exhibited near-complete loss of KPNA5 binding, including F134A/M136A (cluster 1A mut), R137A/T138A/Q139A (cluster 1C mut), Q184A/N185A/H186A/R137A/T138A (cluster 2 mut + R137A/T138A), and L201A/E203A/P204A/D205A/S207A (cluster 3 mut), although the latter two mutants were expressed to lower levels compared to other eVP24s (Figures 3C, 3D, and S3). All residues selected in these multiple mutants, with the exception of cluster 1A mut, were direct contact residues that were observed within 5 Å of KPNA5C in the structure. These results suggest that the high-affinity interaction surface on eVP24 spans several loop regions and, with the exception of R137A, multiple mutations are necessary to obtain near-complete loss of binding.

Residues Specific to NPI-1 Subfamily of KPNAs Make Critical Interface Contacts

There are 12 residues of KPNA5 that form nonbonded contacts with eVP24 in the structure of the eVP24/KPNA complex. From these, we selected a representative subset of residues that included residues conserved among the six human KPNAs (E474, D480, and E483) and a few residues that are identical only in the NPI-1 subfamily of KPNAs (R398, D431, Y477, F484, and S487) (Figure S3B). Most KPNA5 single-residue mutants minimally impacted the interaction with eVP24 (Figure 3E). However, the following four mutants are the notable exceptions: R398A, Y477A, Y477G, and F484A (Figures 3E and 3F). Y477 was implicated previously as an important residue for PY-STAT1 binding with quantitative binding studies showing >20-fold lower binding affinity to KPNA1 (Nardozzi et al., 2010). In the structure of the complex, Y477 of KPNA5C makes extensive nonbonded contacts with eVP24. The binding of eVP24 to Y477A and Y477G shows partial loss of binding in coIP experiments, and the level of attenuation appears to correspond to the hydrophobicity of the side chain (Figure 3G). We also mutated several
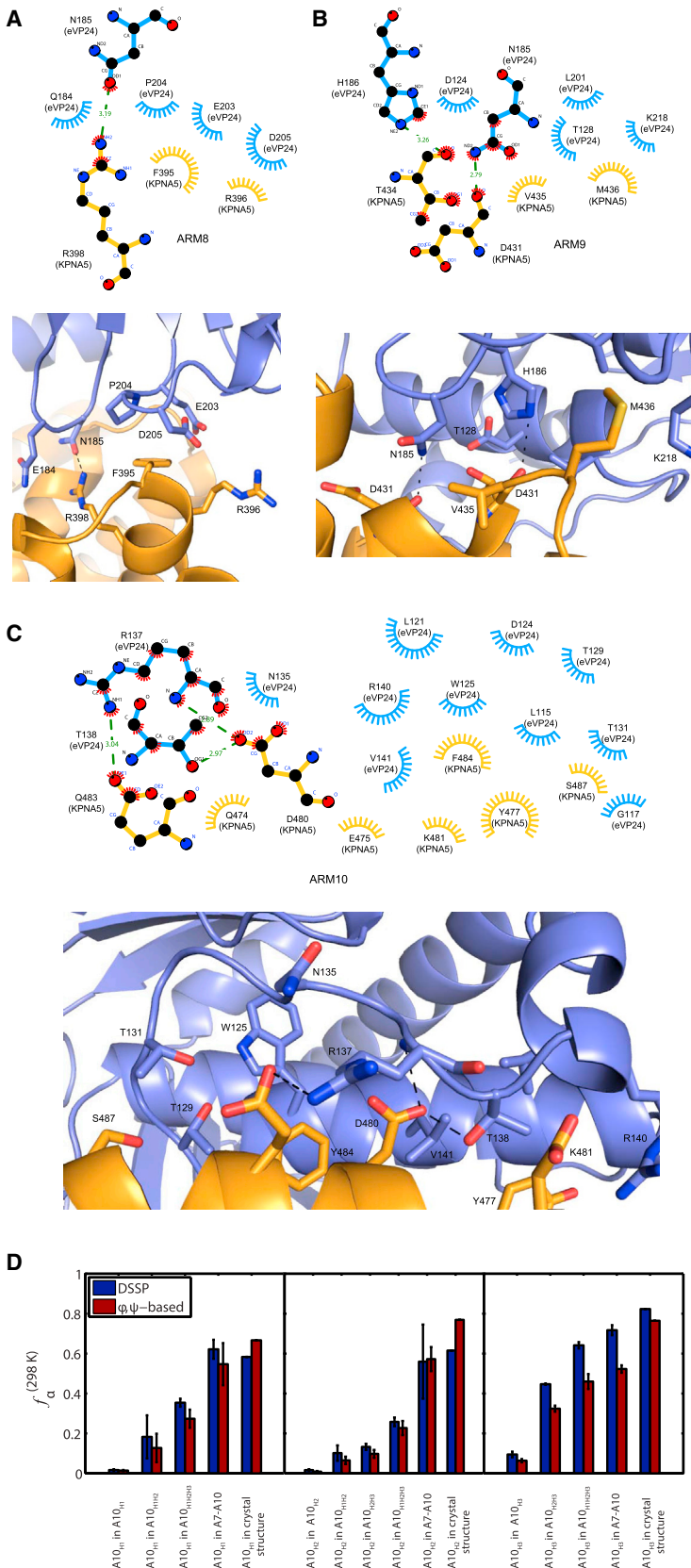
Figure 2. The eVP24 and KPNA5 Interface Reveals Extensive Interactions

(A–C) Extensive hydrogen bonding and hydrophobic interactions are observed between eVP24 and KPNA5 ARM 8 (A), ARM 9 (B), and ARM 10 (C). LigPlot+ diagrams (top) showing protein-protein interactions between eVP24 and KPNA5. Protein side chains are shown as ball and sticks. Hydrogen bonds are shown as green dotted lines. Spoked arcs represent nonbonded contacts. PyMOL representation of the highlighted protein-protein interactions is shown on the bottom. A total of 2,100 Å^2 is covered between the two molecules.

(D) Intrinsic and context-dependent α-helical propensities of KPNA5 ARM helices H1, H2, and H3. The ordinate shows the value of f_α ($0 \leq f_\alpha \leq 1$) at 298 K. The error bars refer to the SEM.
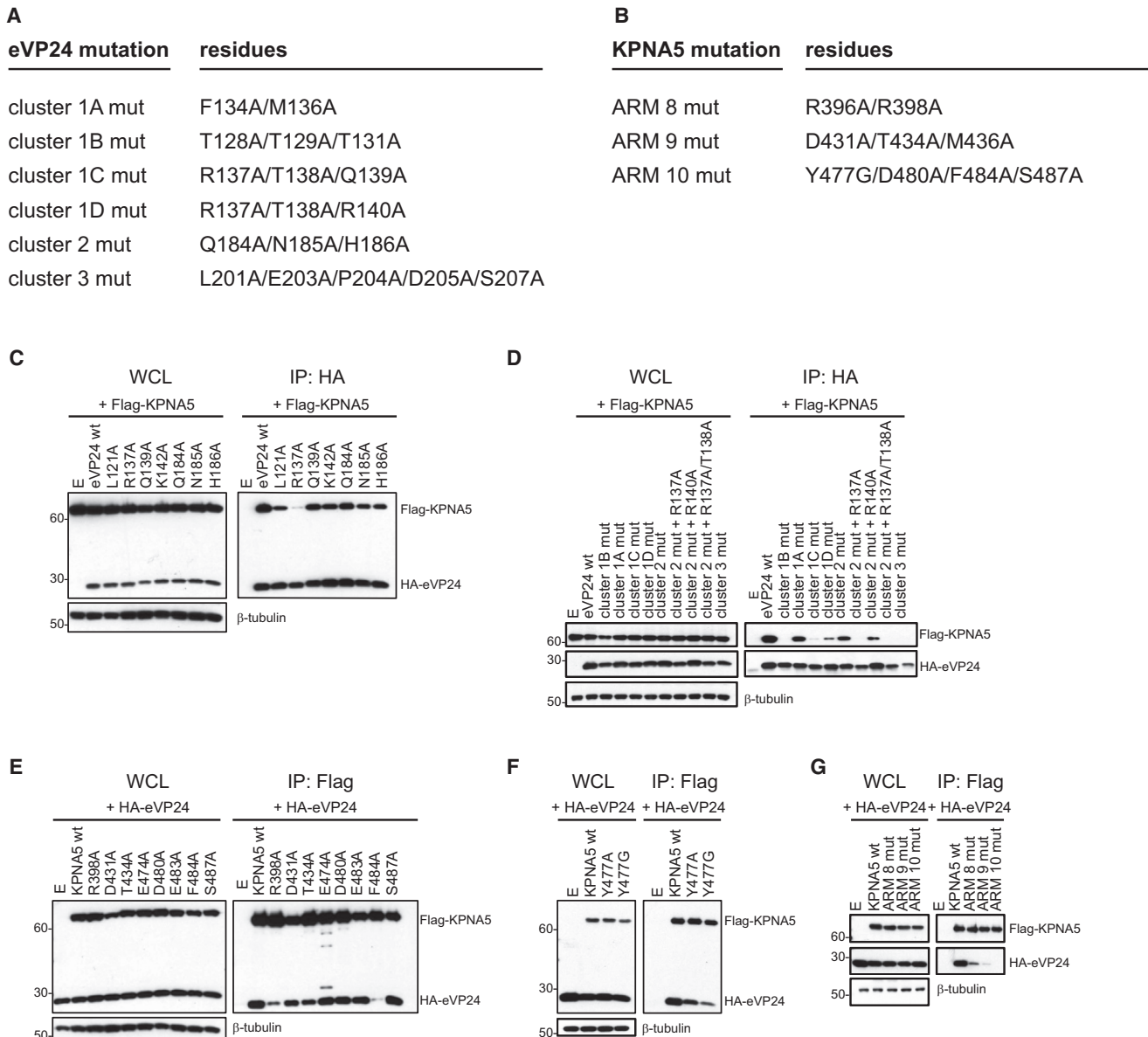
See also Figure S2.

Figure 3. Multiple Residues from KPNA5 ARMs 8–10 Are Necessary and Sufficient for eVP24 Binding
(A) Summary of eVP24 mutants, which were grouped based on the three main residue clusters.
(B) Summary of KPNA5 mutants used in the study, grouped based on their location on the ARM repeats 8–10.
(C and D) CoIP experiments, precipitating with anti-HA antibody, were performed on lysates from 293T cells cotransfected with plasmids for Flag-KPNA5 and HA-eVP24 single-residue (C) or multiple-residue (D) eVP24 mutants as indicated.
(E–G) CoIPs with Flag antibody were carried out on lysates cotransfected with HA-eVP24 WT and Flag-KPNA5 (E) single-residue KPNA5 mutants, (F) at residue Y477 in the ARM 10 hinge, or (G) multiple-residue KPNA5 mutants as indicated. Western blots were performed for Flag, HA, and β-tubulin. WCL, whole-cell lysate; E, pCAGGS empty vector control.
See also Figures S3 and S4.

groups of residues within KPNA5. R396A/R398A (ARM 8 mut), D431A/T434A/M436A (ARM 9 mut), and Y477G/D480A/F484A/S487A (ARM 10 mut) all showed near-complete loss of binding (Figures S3A and 3G). In vitro pull-down assays between KPNA5C and eVP24 confirmed that ARMs 8–10 are necessary for binding using *E. coli*-expressed proteins. These studies also confirmed that the eVP24 residues critical for full-length

KPNA5 binding are also important for binding to the truncated KPNA5C protein (Figure S4), further supporting the notion that the minimal eVP24 binding domain in KPNA5 resides within residues in ARMs 8–10. Collectively, these data are also consistent with the observed combined buried surface area of >2,000 Å^2 and support the hypothesis that eVP24 and KPNA5 share a unique binding interface.
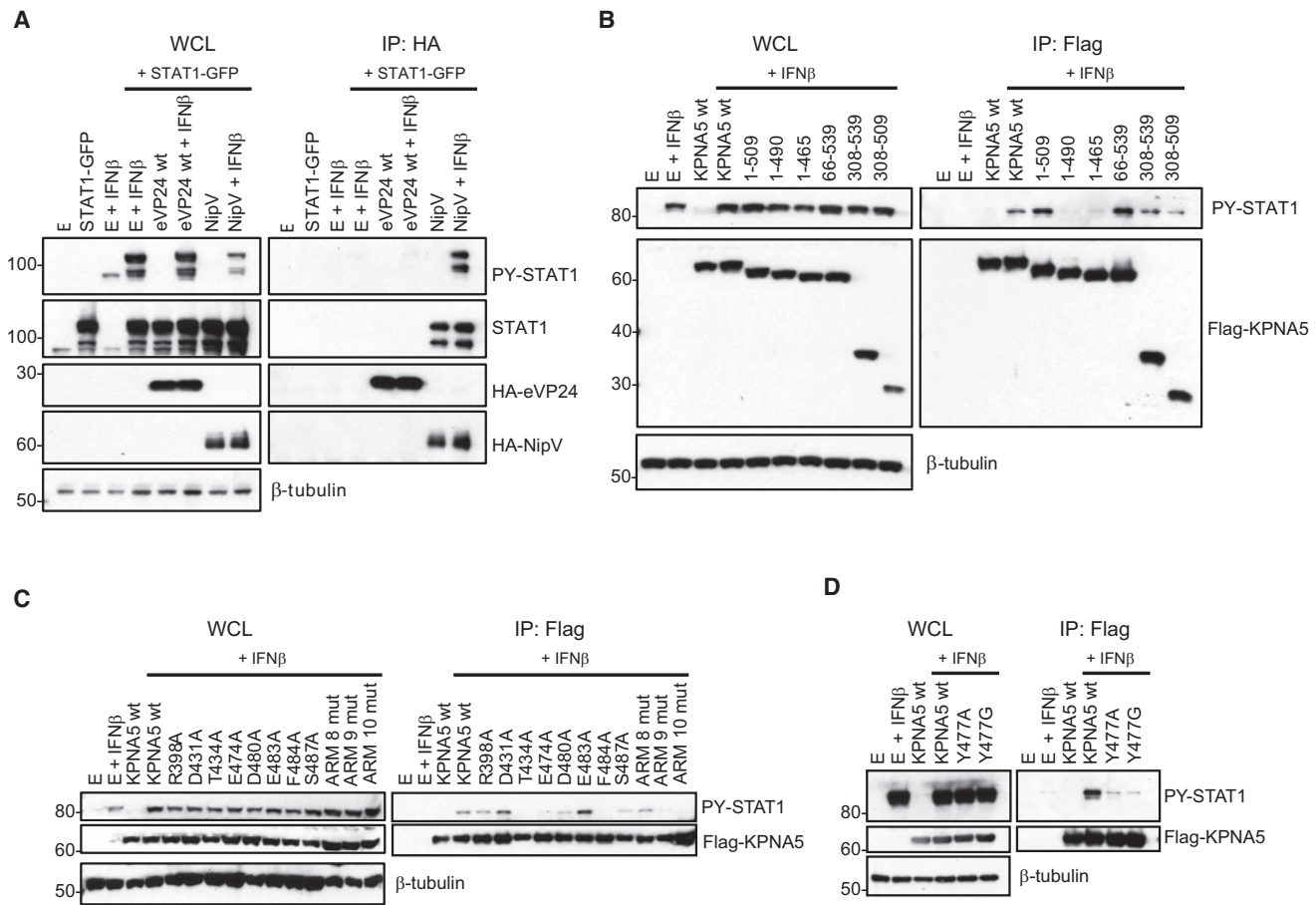
Figure 4. eVP24 and PY-STAT1 Share an Overlapping Binding Site on KPNA5

(A–D) 293T cells were treated with human IFNβ (1000 U/ml) for 30 min. CoIPs with HA or Flag antibody were performed as indicated on the 293T cell lysates transfected with (A) HA-tagged eVP24 or Nipah virus V protein (NipV), (B) KPNA5 truncation mutants, (C) KPNA5 single- and multiple-residue mutants from the eVP24/KPNA5C structural interface, and (D) KPNA5 Y477 single mutants. Western blots were performed for PY-STAT1, STAT1, and Flag or HA. WCL, whole-cell lysate; E, pCAGGS empty plasmid transfection. See also Figure S1.

eVP24 and PY-STAT1 Share a Binding Site on KPNA5

To clarify the extent to which the large interface occupied by eVP24 on KPNA overlaps with the PY-STAT1 binding site, mutant KPNA5 proteins were tested for eVP24 and PY-STAT1 binding. Coprecipitation experiments show that eVP24 does not detectably interact with STAT1 in either its unphosphorylated or tyrosine-phosphorylated form, whereas Nipah virus V (NiV) protein, a known STAT1 binder, readily interacted with STAT1-GFP and PY-STAT1-GFP (Figure 4A) (Ciancanelli et al., 2009; Reid et al., 2006). Analogous experiments examining interaction with endogenous STAT1 also detected NiV V-STAT1 interaction but did not detect eVP24-STAT1 interaction (data not shown). These results suggest that direct binding to STAT1 is unlikely to explain the inhibitory effects of eVP24 on STAT1 signaling. The C terminus of KPNA5, including the eVP24 binding site of ARMs 8–10, was required for PY-STAT1 interaction (Figure 4B). The extreme C-terminal region of KPNA5 (residues 510–539) also appears to be important for PY-STAT1 binding, as the truncation mutants of KPNA lacking residues 510–539 show reduced PY-STAT1 binding. These observations are consistent with previous observations suggesting an extensive binding interface

between PY-STAT1 and KPNA (Nardozzi et al., 2010; Reid et al., 2007). However, these previous studies did not definitively identify the specific ncNLS binding site on KPNA or the ncNLS of PY-STAT1. Additionally, several single-residue mutants (T434A, E474A, Y477A, Y477G, and F484A) in KPNA5 attenuated or abolished binding to PY-STAT1 (Figures 4C and 4D). For example, the Y477G mutation in KPNA5 leads to near-complete loss of binding (Figure 4D). In non-NPI-1 subfamily KPNA proteins, the residue corresponding to Y477 in the structure is glycine, suggesting that this residue may play an important role in determining binding specificity. These results support a model where the KPNA5-eVP24 binding interface on KPNA5 overlaps, at least partially, with the ncNLS binding site for PY-STAT1, setting up a direct competition between eVP24 and PY-STAT1 for the NPI-1 subfamily KPNA binding during viral infections.

eVP24 Binding Interface Mutants Show Diminished Inhibition of PY-STAT1 Nuclear Transport

Next, we assessed the functional impact of eVP24 binding to KPNA5C on STAT1-mediated nuclear transport and signaling. Addition of IFNβ to empty vector-transfected cells triggered
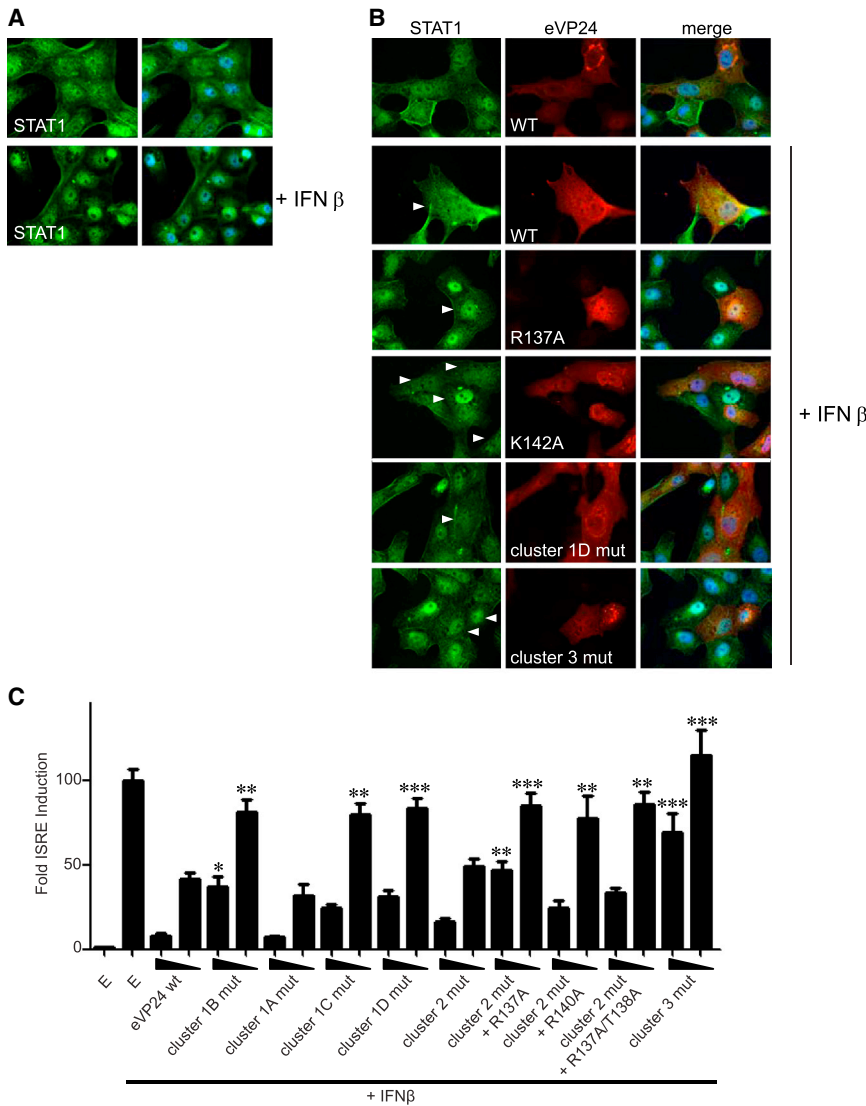
Figure 5. Recognition of a Shared ncNLS Binding Site on KPNA by eVP24 Is Important for Inhibiting PY-STAT1 Nuclear Localization and ISG Induction

(A and B) eVP24/KPNA5 interface mutants R137A and cluster 3 mut fail to inhibit IFN-mediated STAT1 nuclear translocation. (A) Vero cells were untreated or mock treated with IFNβ for 30 min to induce STAT1 nuclear localization (empty plasmid [E] + IFNβ). (B) Ectopic expression of eVP24 WT or mutants differentially affects PY-STAT1 translocation to the nucleus after IFNβ treatment. White arrows highlight IFNβ-treated cells that also express eVP24 WT or eVP24 mutants. Representative data from one of two independent experiments is shown.

(C) The ability of eVP24 to inhibit induction of the ISG54 promoter was assessed. 293T cells were cotransfected with an ISG54 firefly luciferase reporter, a constitutively expressed *Renilla* luciferase plasmid, and the indicated eVP24 expression plasmids. The values represent the mean and SEM of six samples, and statistical significance was assessed by a one-way ANOVA comparing individual mutants to the corresponding eVP24 WT transfection, where ***$p < 0.001$, **$p < 0.01$, and *$p < 0.05$. E, pCAGGS empty plasmid transfection. (D) eVP24 competes with PY-STAT1 for binding to KPNA5. FLAG-KPNA5 was used to coIP PY-STAT1 in the presence or absence of eVP24 or mutants with attenuated KPNA5 binding. Two concentrations (2 and 4 μg) of eVP24 plasmids were tested. E, pCAGGS empty plasmid transfection.

mutants exhibiting impaired KPNA5 binding. Consistent with its lower impact on eVP24-KPNA5 binding, the eVP24 K142A mutant only partially inhibited PY-STAT1 nuclear accumulation, whereas mutants that abolish binding show a corresponding near-complete loss of inhibitory activity against PY-STAT1 nuclear localization (Figure 5B). Collectively, these results suggest that direct binding of eVP24 to NPI-1 subfamily of KPNAs likely explains the inhibition of PY-STAT1 nuclear import in EBOV-infected cells that was previously observed by Reid et al. (2006).

eVP24 WT, But Not Interface Mutants, Can Successfully Block ISRE Activity

STAT1 phosphorylation is required for type I and II IFN responses. Specifically, the type I IFNs provide cell-intrinsic innate immunity through the induction of ISRE genes that results in an antiviral state. Therefore, we tested the ability of eVP24 wild-type (WT) or eVP24 interface mutants to inhibit activation of the ISG54 promoter using dual reporter assays. As expected, eVP24 WT inhibits ISRE induction, while cluster 1 and cluster 3 mutants with impaired KNPA5 binding exhibited a corresponding loss

nuclear accumulation of STAT1 (Figure 5A), whereas expression of eVP24 inhibited STAT1 relocalization. Using a similar assay, we tested eVP24 mutants with reduced KPNA5 binding activity, including R137A, K142A, cluster 1D mut, and cluster 3 mut mutants, in order to assess their ability to inhibit PY-STAT1 nuclear trafficking. Resulting data, shown in Figure 5B, reveal reduced inhibition of PY-STAT1 translocation in response to IFNβ by eVP24

of inhibitory activity in the ISRE assay (Figure 5C). However, despite making several contacts with KPNA5, cluster 2 displayed WT levels of ISRE activity, suggesting that this region is not important for function. Among individual mutants, R137A and R140A appear to display the highest impact on ISRE activity. Similarly, cluster 3 mutants show the highest level of activity loss. The correlation between the level of ISRE induction and the ability of eVP24 mutants to bind KPNA further support a model where eVP24 binding to KPNA limits PY-STAT1 nuclear localization, resulting in the inhibition of cell-intrinsic innate immune signaling.

eVP24 Competes with PY-STAT1 for KPNA Binding

A combination of the eVP24/KPNA5C complex structure and the biochemical analysis of the binding interface described above suggest that the eVP24 binding site on KPNA5 partially overlaps with the PY-STAT1 binding site. Our measured affinity for KPNA5 with eVP24 is in the low nanomolar range (K_D = 1–10 nM for eVP24/KPNA5) (Figure 1B). In a similar experiment, we observe that PY-STAT1 binds KPNA5 with a micromolar dissociation constant, which is about 1000-fold weaker (Figure S6A). In agreement with these studies, we were unable to observe measureable binding activity between KPNA5 and unphosphorylated STAT1 (U-STAT1) (Figure S6A). A previous study reported that PY-STAT1 bound to KPNA1 with a K_D ranging from 150–191 nM (Nardozzi et al., 2010), approximately 30-fold less than KPNA1/5 binding to eVP24. The observed differences are likely due to changes in the experimental conditions or may reflect the specificities between KPNA1 and KPNA5 for binding to PY-STAT1.

Next, we tested the direct competition model by assessing the ability of eVP24 WT to block KPNA5 interaction with PY-STAT1. As shown in Figure 5D, eVP24 WT protein exhibited near-complete inhibition of KPNA5 interaction with PY-STAT1. eVP24 R137A, which exhibits reduced but measurable KPNA5 binding, displayed a slightly diminished dose-dependent inhibitory activity toward the interaction between PY-STAT1 and KPNA5. In contrast, two eVP24 mutants, cluster 1D mut and cluster 3 mut, which showed greatly reduced KPNA5 binding in coIP assays, displayed a significantly diminished ability to block the interaction at the concentrations tested (Figure 5D). These competition assays, where eVP24 (or eVP24 mutants) and PY-STAT1 have equal probability to interact with KPNA, further support a model where inhibition of PY-STAT1 nuclear localization by eVP24 is due to direct competition by eVP24 for NPI-1 subfamily KPNA binding.

eVP24 and cNLS Cargo Occupy Independent Binding Sites on NPI-1 Subfamily KPNAs

Nucleocytoplasmic trafficking is important for normal cellular processes and for responses to extracellular stimuli. Previous studies have shown that PY-STAT1, produced in response to type I IFNs, can bind KPNAs independent of cNLS cargo binding (Melen et al., 2003; Sekimoto et al., 1997) (Figures 6A and 6B). To test whether eVP24 and cNLS cargo occupy independent binding sites on KPNA5, we conducted two sets of experiments. First, we tested the ability of cNLS cargo to associate with and translocate into the nucleus through KPNA association. In order to overcome potential redundancy of KPNAs for cNLS-containing cargo, we specifically tested the ability of eVP24 to affect KPNA interaction with deleted in breast cancer 1 (DBC1) protein,

which uses a validated basic cNLS to associate with KPNA1 and KPNA5 and mediate its nuclear import (Wälde et al., 2012). As shown in Figure 6C, Myc-tagged DBC1 can associate with KPNA1 and KPNA5. The presence of increasing levels of eVP24 does not appear to inhibit DBC1 association with KPNA1 or KPNA5. Therefore, these results suggest that the cNLS binding site for DBC1 and the eVP24 binding site, which is a ncNLS binding site on NPI-1 subfamily KPNAs, are separate.

As a quantitative test of the model, where cNLS and the ncNLS binding site for PY-STAT1 and eVP24 on NPI-1 subfamily KPNA is distinct, we conducted competition ITC experiments for several cNLS peptide/KPNA combinations in the presence or absence of eVP24. Specifically, we tested monopartite cNLS (SV40 peptide) binding to KPNA1 or bipartite cNLS cargo (nucleoplasmin peptide) binding to KPNA1 and KPNA5 (Figures S6B–S6E). Comparison of KPNA1 alone with KPNA1 in a 1:1 complex with eVP24 reveals that for cNLSs, such as SV40, or for cargo, such as DBC1, the binding sites for cNLS and ncNLS for PY-STAT1/eVP24 are distinct (Figure S6C). Similarly, our data for the bipartite cNLS also confirm that the eVP24 binding to KPNA1 or KPNA5 does not significantly impact cNLS binding (Figures S6D and S6E). However, we do observe a 2-fold difference for nucleoplasmin bipartite NLS peptide binding to KPNA1 and KPNA5 in the presence or absence of eVP24. This 2-fold difference is likely due to allosteric effects, as the eVP24 binding site and the minor cNLS binding sites are located in KPNA5 ARM 8. Taken together, these results support a model for distinct binding sites for cNLS and the PY-STAT1-specific ncNLS recognized by eVP24 on KPNA5 (and other NPI-1 subfamily members). Therefore, eVP24, like PY-STAT1, is unlikely to impact nuclear transport of cNLS bearing cargo by KPNA.

eVP24 and the Related mVP24 Display Structural Differences Near the KPNA Binding Residue Clusters

In contrast to eVP24, mVP24 lacks IFN antagonist activity (Valmas et al., 2010). Comparison of the mVP24 and eVP24 sequences suggest that there are major differences in the primary sequence of the three eVP24 clusters, which contribute significantly to KPNA5 binding (Figure S3A). In addition to the differences in their sequence, structural comparisons also reveal significant differences near these clusters between eVP24 and mVP24 (Figure S5), suggesting that the differences in the primary sequence also contribute to structural differences. For example, the region surrounding cluster 3 shows the most apparent structural change, where the mVP24 structure (Zhang et al., 2014) shows an extended antiparallel β strand connected by a short loop; the corresponding region in eVP24 consists of two short antiparallel β strands connected by linkers and a short α helix (Figure S5) (Edwards et al., 2014; Zhang et al., 2012b). Thus, sequence and structural differences near key clusters of eVP24 that are important for KPNA5 interaction likely explain the differences in observed IFN-signaling antagonist properties between EBOV and MARV VP24 proteins.

DISCUSSION

Innate immune responses to pathogens can dictate the outcomes of infections. During outbreaks, EBOV infections result in high case fatality rates in part due to virally encoded immune

CellPress
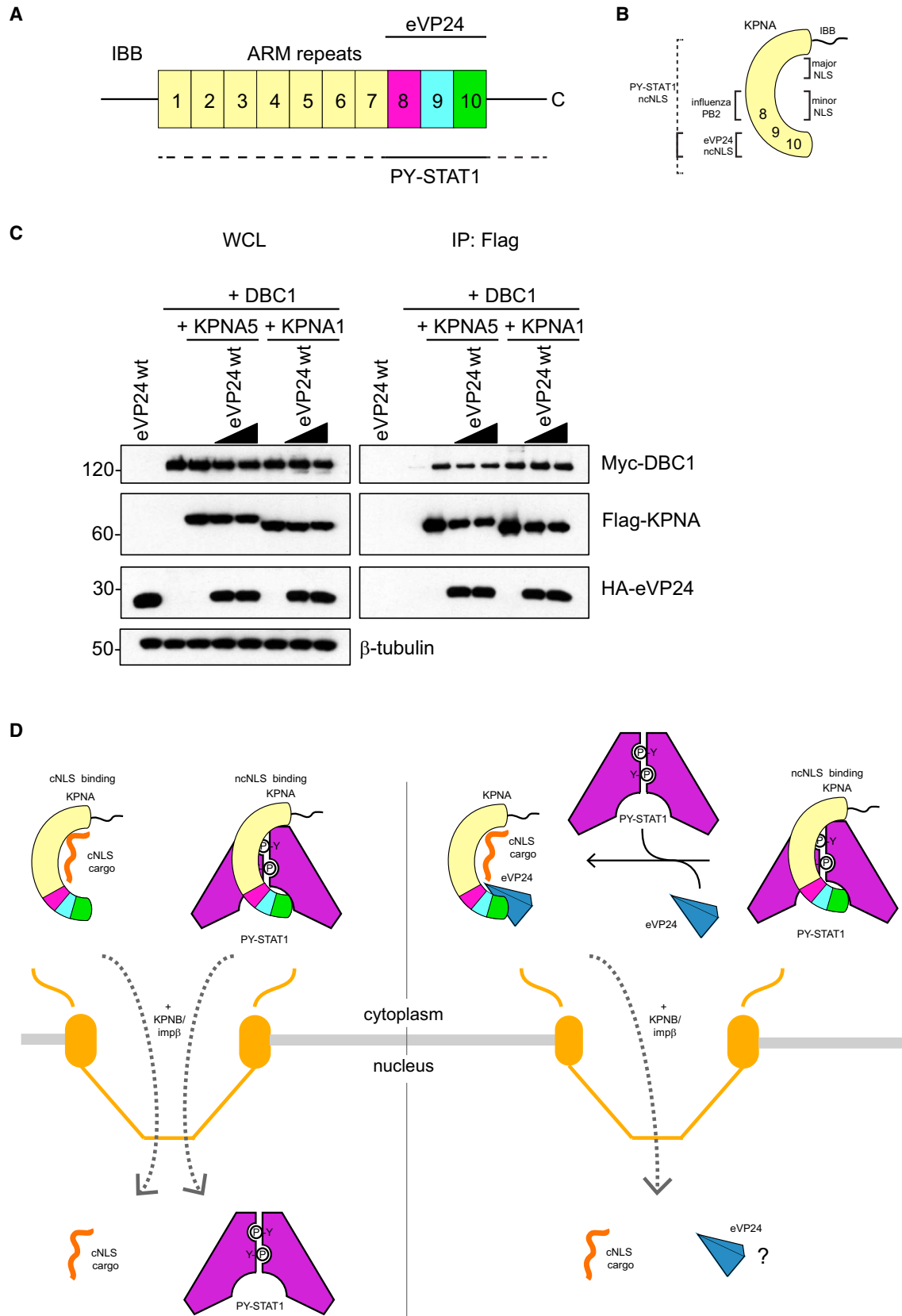
antagonists. In addition to virally encoded inhibitors of type I IFN production, such as filoviral VP35 proteins, EBOV infections are also refractory to type I and II IFN treatments. Type I and II IFNs activate antiviral responses through JAK/STAT signaling. In the JAK/STAT signaling pathway, a key committal step is the phosphorylation and nuclear translocation of STAT1, which can form either homodimers with another molecule of PY-STAT1 or heterodimers with STAT2. In each of these pathways, PY-STAT1 and nuclear translocation via NPI-1 subfamily KPNAs is important for antiviral gene expression. The use of a unique ncNLS binding site on these KPNAs by the host provides a mechanism for rapid recruitment of PY-STAT1-associated transcription complexes to the nucleus. It is likely that this ncNLS-mediated import of PY-STAT1 is independent of normal nuclear transport, which is typically coordinated through the direct recognition of a cNLS by KPNAs. Through a combination of structural and biochemical approaches, we define the molecular basis for eVP24-mediated inhibition of cell-intrinsic immune responses and describe a key molecular determinant that is important for PY-STAT1 transport (summarized in Table S1 and Figure 6B). A previous study using in vitro binding assays reported that U-STAT1 can also bind to eVP24, suggesting an alternate mechanism by which eVP24 may limit nuclear STAT1 (Zhang et al., 2012b). Our cell-based data (see Figure 4A) as well as previous studies by Reid et al. (2006) and Pichlmair et al. (2012) do not support this model proposed by Zhang et al. (2012b). Instead, our data support a model where competitive and preferential binding of eVP24 to the specific nuclear transporters from the NPI-1 subfamily of KPNAs instead of PY-STAT1 results in diminished ISRE activation, which contributes to the observed eVP24-mediated inhibition of cell-intrinsic innate immune signaling, including the resistance of EBOV-infected cells for IFN treatment (Figure 6D).

Although EBOVs and MARVs are closely related and share identifiable genome organization, including similar open reading frames with high sequence similarities, these two genera of viruses also exhibit significant differences. A previous study by Valmas et al. (2010) revealed that unlike eVP24, mVP24 does not inhibit JAK/STAT signaling. Consistent with this observation, our recent studies revealed that mVP24 can activate host antioxidant response element genes, which likely provides additional support for viral growth (Edwards et al., 2014). Evaluation of our results here reveals that the sequences near cluster 1 and cluster 3 are different between these two VP24s. Given the importance of these regions to KPNA binding by eVP24, it is

likely that these regions, specifically those that make direct contact with KPNAs, are important for discrimination. Interestingly, clusters 1 and 3 are highly conserved among different EBOV species. In contrast, cluster 2 residues show limited sequence conservation. These sequence and structural variations between eVP24 and mVP24, together with the structural results from this study, provide a basis by which functional specificity of filoviral VP24 proteins can be defined.

KPNAs are important for transport of NLS-containing cargo. Our proposed model also predicts that the nucleocytoplasmic trafficking of cNLS-containing cargo will be largely unaffected by the binding of eVP24. The overlap in the binding also suggests that PY-STAT1 binding is unlikely to impact normal transport. In contrast to cNLS cargo, the interaction between eVP24 and NPI-1 subfamily KPNAs will specifically inhibit PY-STAT1 nuclear transport and limit the effect of IFNs on EBOV-infected cells. In addition to providing a mechanism for direct inhibition of cell-intrinsic immunity, our model allows us to rationalize how EBOV-infected cells may continue to function normally during initial stages of infection, as the nucleocytoplasmic trafficking of cNLS-containing cargo remain unaffected while JAK/STAT signaling is shut off.

Similar to eVP24, influenza A virus NP and PB2 proteins are also known to interact with KPNA via ncNLSs; however, the functional consequences of these viral binders of KPNA are distinct from eVP24. For example, influenza virus NP and PB2 interact with KPNAs to facilitate viral replication functions, whereas eVP24 inhibits innate immunity. Moreover, the influenza virus proteins display distinct specific binding regions and exhibit different KPNA specificities (Melen et al., 2003; Tarendeau et al., 2007) (Figure S7). Findings from this study, coupled with these previous observations, indicate that different viruses may exploit critical regions on KPNA transporters to enhance viral replication. By targeting the binding site on KPNAs that is critical for PY-STAT1 recognition and nuclear transport, EBOV disables cell-intrinsic antiviral signaling in order to facilitate virus replication without impacting normal cellular cargo transport. Additionally, structural insights from our study also provide the framework for targeting the eVP24/KPNA interface pharmacologically to resensitize Ebola virus to IFNs.

EXPERIMENTAL PROCEDURES

Constructs

eVP24 (NCBI accession number AGB56798.1) and KPNA5 (NCBI accession number NP_002260.2) cDNAs were used as templates to subclone eVP24

Figure 6. Model of eVP24 Inhibition of KPNA-Mediated STAT1 Signaling

(A) Schematic diagram illustrating the domain organization of KPNA containing an N-terminal importin β binding (IBB) domain followed by 10 ARM repeats, each of which is comprised of 3 α helices (H1, H2, and H3), and a short C terminus. eVP24 and STAT1 bind overlapping sites in ARMS 8–10 (highlighted in red, blue, and green). Overlapping binding site between eVP24 and KPNA5 is shown as a solid black line, and the additional regions potentially important for PY-STAT1 binding are shown as a black dotted line.

(B) Relative locations of cNLS and ncNLS sites based on available data, including the current study.

(C) CoIP experiments with Flag antibody were performed on lysates of 293T cells cotransfected with either Flag-KPNA1 or Flag-KPNA5 and Myc-DBC1 and concentrations of 2 and 4 μg of HA-eVP24 as indicated. Western blots were performed on precipitated (IP) material and on whole-cell lysates (WCLs) for HA, Myc, and Flag tags.

(D) Model of KPNA (PDB ID: 1BK5) in cylinder representation. The major and minor nuclear localization signals (NLSs) span the inner surface of ARMs 2–4 and ARMs 6–8, respectively. The ncNLS used by PY-STAT1 or the KPNA binding site of eVP24 is independent of the cNLS sites. Therefore, KPNA loaded with PY-STAT1 ± cNLS cargo can translocate into the nucleus. In contrast, eVP24 binding, via a portion of the region used by PY-STAT1 via ARMs 8–10, inhibits PY-STAT1 nuclear translocation, but not the transport of cNLS containing cargo.

See also Figures S6 and S7 and Table S1.

constructs into a modified maltose binding protein (MBP) fusion containing pET15b vector (Novagen). Mutations were generated using the overlap PCR method and verified by sequencing.

Protein Expression and Purification
eVP24 and KPNA5 constructs were ectopically expressed in BL21(DE3) *E. coli* cells (Novagen) in Luria Broth media. Protein expression was induced at an OD_{600} (optical density at 600 nm) of 0.6 with 0.5 mM IPTG and grown for 12–15 hr at 18°C.

eVP24 and KPNA5 Constructs
Cells were harvested, resuspended in lysis buffer (buffer L) containing 25 mM sodium phosphate (pH 7.5), 250 mM NaCl, 20 mM imidazole, and 5 mM 2-mercaptoethanol (BME), lysed using an EmulsiFlex-C5 homogenizer (Avestin), and clarified by centrifugation at 30,000 × *g* at 4°C for 30 min. Proteins were purified using a series of affinity and ion-exchange chromatographic columns. Following TEV protease digestion to remove the MBP tag, the resulting sample was further purified using ion-exchange chromatography to isolate the protein of interest from the MBP fusion prior to application on a size exclusion column.

eVP24/KPNA5C Complex
Purified eVP24 and KPNA5C were mixed with a 1:1.5 ratio followed by size exclusion chromatography on a Superdex 75 column (GE Healthcare). The complex was verified by SDS-PAGE and concentrated to 8 mg/ml. Crystals were grown by streak seeding into 3.5 M ammonium chloride and 0.1 M Bis-Tris propane (pH 7.0) at 20°C by vapor diffusion.

STAT1 Constructs
All STAT1 constructs were cloned into pET23b with a C-terminal 6xHis-tag or pET15b and ectopically expressed in BL21(DE3) *E. coli* cells (Novagen) in LB media. Protein expression was induced at an OD_{600} of 0.6 with 0.5 mM IPTG and grown for 12–15 hr at 18°C and purified using methods similar to those for eVP24 purification.

EGFR Intracellular Domain
Sf9 insect cells growing in Sf900 III media (Gibco) and 1:100 antibiotic antimycotic (Gibco) were infected with baculovirus (1:100) containing EGFR construct (kind gift from Dr. Bose). At 72 hr postinfection, cells were harvested, resuspended in buffer L, lysed with a Dounce homogenizer (20 passes), and clarified by centrifugation at 50,000 × *g* for 40 min at 10°C. EGFR was purified using a nickel affinity column (GE Healthcare).

PY-STAT1
Kinase reactions were carried out following modified conditions previously described by Vinkemeier et al. (1996). Briefly, STAT1 at 1 mg/ml in 20 mM Tris (pH 7.0), 150 mM NaCl, 400 μM ATP, 10 mM MnCl₂, 10 mM 2-beta-mercaptoethanol, and 0.04 mg/ml EGFR was incubated at 30°C with no agitation for 2–4 hr, and the reactions were quenched with 10 mM EDTA (final) or by direct loading onto a heparin column. PY-STAT1 was further purified by heparin affinity and size exclusion chromatography (GE Healthcare) prior to use.

Data Collection and Structure Determination
Crystals were screened at Advanced Photon Source Beamline 19ID and at the Advanced Light Source Beamline 4.2.2. Diffraction images were collected at a crystal-to-detector distance of 300 mm, and the data were processed by HKL3000 (Otwinowski and Minor, 1997). PDB ID 4M0Q was used as a search model, and the KPNA5C residues were built by three cycles of Bucanneer (CCP4i) (Winn et al., 2011), manual model building in COOT (Emsley and Cowtan, 2004), and refinement with REFMAC5 (Collaborative Computational Project, Number 4, 1994) or PHENIX1.8.4 (Adams et al., 2010). The structure quality was assessed with MolProbity (Davis et al., 2007).

Coprecipitation Assays
At 24 hr posttransfection with plasmids as indicated in the figure legends, human embryonic kidney 293T (HEK293T) cells were lysed in NP-40 lysis buffer (50 mM Tris [pH 7.5], 280 mM NaCl, 0.5% Nonidet P-40, 0.2 mM EDTA, 2 mM EGTA, 10% glycerol, protease inhibitor [cOmplete; Roche]) and phosphatase inhibitor (PhosSTOP; Roche). For PY-STAT1 coIPs, HEK293T cells were first treated with 1000 U/ml human IFNβ (PBL) in Dulbecco's modified Eagle's medium (DMEM), 0.3% BSA for 30 min before lysis. Anti-FLAG M2 magnetic beads or anti-HA beads (Sigma-Aldrich) were incubated with lysates for 1 hr

at 4°C, washed five times in NP-40 lysis buffer, and eluted using either 3X FLAG peptide (Sigma-Aldrich) or by boiling in sample loading buffer.

Isothermal Titration Calorimetry
Binding assays were performed on a VP-isothermal titration calorimeter (VP-ITC) (Microcal). Protein samples were dialyzed against buffer (10 mM HEPES [pH 7.0], 150 mM NaCl, and 2 mM TCEP) for 12 hr at 25°C. Titrations were set up with 50–100 μM protein in the syringe and 4–10 μM protein in the cell. For competition studies such as those in Figure S6, the complex of 1:1 was used. A reference power of 4 μcal/s and the resulting ITC data were processed and fit to a one-site binding model to determine n (number of binding sites) and K_D (dissociation constant) using ORIGIN 7.0 software. All experiments were performed at least in duplicate.

In Vitro Pull-Down Assays Using Recombinantly Expressed Proteins
Amylose resin was pre-equilibrated with buffer (20 mM Tris [pH 7.5], 150 mM NaCl, 5 mM BME) prior to the addition of lysate containing recombinantly expressed MBP-tagged proteins at 4°C. Resin was incubated for 10 min, followed by washes and subsequent resuspension. Purified KPNA5C or VP24 proteins were applied to the resin and allowed to incubate for 20 min, prior to washes and final resuspension in buffer. Samples were taken at each step and visualized by Coomassie blue staining of SDS-PAGE.

Reporter Gene Assay
HEK293T cells were transfected with an ISG54 firefly luciferase reporter plasmid, a constitutively active *Renilla* luciferase reporter plasmid (pRL-tk; Promega), and the indicated protein expression plasmids. At 24 hr posttransfection, the cells were treated with 1,000 U/ml human IFNβ (PBL) in DMEM, 10% fetal bovine serum. At 24 hr posttreatment, a dual luciferase reporter assay (Promega) was performed, and firefly luciferase values were normalized to *Renilla* luciferase values. Statistical significance was assessed by a one-way ANOVA using Student's t test for comparisons as indicated.

Antibodies
Monoclonal mouse anti-FLAG M2 antibody, polyclonal rabbit anti-Flag antibody, monoclonal mouse anti-HA antibody, and a polyclonal rabbit anti-HA antibody were purchased from Sigma-Aldrich. Anti-STAT1 and anti-STAT1 (pY701) were purchased from BD Transduction Laboratories.

Computational Analysis
Atomistic Metropolis Monte Carlo simulations based on the ABSINTH implicit solvation model (Vitalis and Pappu, 2009) were used to quantify the intrinsic and context-dependent α-helical propensities of ARM10 helices H1, H2, and H3. This quantity is calculated using hydrogen-bonding criteria as implemented in the DSSP algorithm (Kabsch and Sander, 1983) and an assessment of backbone ϕ and ψ angles. For example, $A10_{H1}$ in $A10_{H1H2}$ refers to the helicity of segment H1 of the ARM10 repeat quantified in a simulation that includes only segments H1 and H2, respectively, whereas $A10_{H1}$ in $A10_{H1H2H3}$ refers to the helicity of segment H1 of the ARM10 repeat quantified in a simulation that includes segments H1, H2, and H3 of ARM10.

STAT1 Nuclear Translocation Assays
The assay was performed as described previously (Reid et al., 2006). Briefly, Vero cells were seeded onto 12 mm diameter glass coverslips and transfected with empty vector (pCAGGS), VP24 HA (pCAGGS), or VP24 HA mutants (pCAGGS) using Lipofectamine 2000 (Life Technologies). At 24 hr posttransfection, cells were serum starved for 4 hr and then either mock treated or treated with 1,000 U/ml of human IFNβ for 30 min at 37°C. Cells were rinsed twice with PBS containing calcium chloride and magnesium chloride (PBS-CM), fixed with 4% parformaldehyde for 30 min, and blocked for 45 min at room temperature (RT) with 4% normal goat serum in PBS containing 0.5% BSA and 0.15% glycine (PBG). Subsequently, coverslips were incubated with rabbit anti-STAT1 (5 μg/ml; Santa Cruz) and mouse anti-HA (1:200) for 1 hr at RT. Coverslips were rinsed and incubated with Alexa 488-conjugated goat antibody raised against rabbit immunoglobulin G (IgG), Alexa 555-conjugated antibody raised against mouse IgG, and Hoechst 33342 (Invitrogen). Images were acquired using an AxioPlan2 fluorescent microscope.

CellPress

Structural Figure Generation and Analysis

Surface area and surface complementarity were calculated using AREAIMOL and Sc, respectively, as implemented in the CCP4 program suite (Collaborative Computational Project, Number 4, 1994). Structure figures were prepared using PyMOL (DeLano, 2002). Protein-protein interactions were analyzed using LigPlot[+] (Laskowski and Swindells, 2011). Topology diagrams were generated by PDBSum (Laskowski, 2007).

ACCESSION NUMBERS

Coordinates and structure factors have been deposited in the Protein Data Bank under PDB ID 4U2X.

SUPPLEMENTAL INFORMATION

Supplemental Information includes seven figures and one table and can be found with this article online at http://dx.doi.org/10.1016/j.chom.2014.07.008.

REFERENCES

Adams, P.D., Afonine, P.V., Bunkóczi, G., Chen, V.B., Davis, I.W., Echols, N., Headd, J.J., Hung, L.W., Kapral, G.J., Grosse-Kunstleve, R.W., et al. (2010). PHENIX: a comprehensive Python-based system for macromolecular structure solution. Acta Crystallogr. D Biol. Crystallogr. 66, 213–221.

Basler, C.F., and Amarasinghe, G.K. (2009). Evasion of interferon responses by Ebola and Marburg viruses. J. Interferon Cytokine Res. 29, 511–520.

Bray, M., and Murphy, F.A. (2007). Filovirus research: knowledge expands to meet a growing threat. J. Infect. Dis. 196 (Suppl 2), S438–S443.

Chen, X., Vinkemeier, U., Zhao, Y., Jeruzalmi, D., Darnell, J.E., Jr., and Kuriyan, J. (1998). Crystal structure of a tyrosine phosphorylated STAT-1 dimer bound to DNA. Cell 93, 827–839.

Chook, Y.M., and Blobel, G. (2001). Karyopherins and nuclear import. Curr. Opin. Struct. Biol. 11, 703–715.

Ciancanelli, M.J., Volchkova, V.A., Shaw, M.L., Volchkov, V.E., and Basler, C.F. (2009). Nipah virus sequesters inactive STAT1 in the nucleus via a P gene-encoded mechanism. J. Virol. 83, 7828–7841.

Collaborative Computational Project, Number 4 (1994). The CCP4 suite: programs for protein crystallography. Acta Crystallogr. D Biol. Crystallogr. 50, 760–763.

Conti, E., and Izaurralde, E. (2001). Nucleocytoplasmic transport enters the atomic age. Curr. Opin. Cell Biol. 13, 310–319.

Conti, E., and Kuriyan, J. (2000). Crystallographic analysis of the specific yet versatile recognition of distinct nuclear localization signals by karyopherin alpha. Structure 8, 329–338.

Conti, E., Uy, M., Leighton, L., Blobel, G., and Kuriyan, J. (1998). Crystallographic analysis of the recognition of a nuclear localization signal by the nuclear import factor karyopherin alpha. Cell 94, 193–204.

Cook, A., Bono, F., Jinek, M., and Conti, E. (2007). Structural biology of nucleocytoplasmic transport. Annu. Rev. Biochem. 76, 647–671.

Davis, I.W., Leaver-Fay, A., Chen, V.B., Block, J.N., Kapral, G.J., Wang, X., Murray, L.W., Arendall, W.B., 3rd, Snoeyink, J., Richardson, J.S., and Richardson, D.C. (2007). MolProbity: all-atom contacts and structure validation for proteins and nucleic acids. Nucleic Acids Res. 35 (Web Server issue), W375–W383.

DeLano, W.L. (2002). The PyMOL Molecular Graphics System. (San Carlos, CA: DeLano Scientific).

Edwards, M.R., Johnson, B., Mire, C.E., Xu, W., Shabman, R.S., Speller, L.N., Leung, D.W., Geisbert, T.W., Amarasinghe, G.K., and Basler, C.F. (2014). The Marburg virus VP24 protein interacts with Keap1 to activate the cytoprotective antioxidant response pathway. Cell Rep 6, 1017–1025.

Emsley, P., and Cowtan, K. (2004). Coot: model-building tools for molecular graphics. Acta Crystallogr. D Biol. Crystallogr. 60, 2126–2132.

Feldmann, H., and Geisbert, T.W. (2011). Ebola haemorrhagic fever. Lancet 377, 849–862.

Geisbert, T.W., Young, H.A., Jahrling, P.B., Davis, K.J., Larsen, T., Kagan, E., and Hensley, L.E. (2003). Pathogenesis of Ebola hemorrhagic fever in primate models: evidence that hemorrhage is not a direct effect of virus-induced cytolysis of endothelial cells. Am. J. Pathol. 163, 2371–2382.

Goodbourn, S., Didcock, L., and Randall, R.E. (2000). Interferons: cell signalling, immune modulation, antiviral response and virus countermeasures. J. Gen. Virol. 81, 2341–2364.

Kabsch, W., and Sander, C. (1983). Dictionary of protein secondary structure: pattern recognition of hydrogen-bonded and geometrical features. Biopolymers 22, 2577–2637.

Kaletsky, R.L., Francica, J.R., Agrawal-Gamse, C., and Bates, P. (2009). Tetherin-mediated restriction of filovirus budding is antagonized by the Ebola glycoprotein. Proc. Natl. Acad. Sci. USA 106, 2886–2891.

Laskowski, R.A. (2007). Enhancing the functional annotation of PDB structures in PDBsum using key figures extracted from the literature. Bioinformatics 23, 1824–1827.

Laskowski, R.A., and Swindells, M.B. (2011). LigPlot+: multiple ligand-protein interaction diagrams for drug discovery. J. Chem. Inf. Model. 51, 2778–2786.

Leung, D.W., Prins, K.C., Basler, C.F., and Amarasinghe, G.K. (2010). Ebolavirus VP35 is a multifunctional virulence factor. Virulence 1, 526–531.

Mateo, M., Reid, S.P., Leung, L.W., Basler, C.F., and Volchkov, V.E. (2010). Ebolavirus VP24 binding to karyopherins is required for inhibition of interferon signaling. J. Virol. 84, 1169–1175.

McBride, K.M., Banninger, G., McDonald, C., and Reich, N.C. (2002). Regulated nuclear import of the STAT1 transcription factor by direct binding of importin-alpha. EMBO J. 21, 1754–1763.

Melen, K., Fagerlund, R., Franke, J., Kohler, M., Kinnunen, L., and Julkunen, I. (2003). Importin alpha nuclear localization signal binding sites for STAT1, STAT2, and influenza A virus nucleoprotein. J. Biol. Chem. 278, 28193–28200.

Meyer, T., Begitt, A., Lödige, I., van Rossum, M., and Vinkemeier, U. (2002). Constitutive and IFN-gamma-induced nuclear import of STAT1 proceed through independent pathways. EMBO J. 21, 344–354.

Nardozzi, J., Wenta, N., Yasuhara, N., Vinkemeier, U., and Cingolani, G. (2010). Molecular basis for the recognition of phosphorylated STAT1 by importin alpha5. J. Mol. Biol. 402, 83–100.

Otwinowski, Z., and Minor, W. (1997). Processing of X-ray diffraction data collected in oscillation mode. Methods Enzymol. *276*, 307–326.

Pichlmair, A., Kandasamy, K., Alvisi, G., Mulhern, O., Sacco, R., Habjan, M., Binder, M., Stefanovic, A., Eberle, C.A., Goncalves, A., et al. (2012). Viral immune modulators perturb the human molecular network by common and unique strategies. Nature *487*, 486–490.

Reich, N.C., and Liu, L. (2006). Tracking STAT nuclear traffic. Nat. Rev. Immunol. *6*, 602–612.

Reid, S.P., Leung, L.W., Hartman, A.L., Martinez, O., Shaw, M.L., Carbonnelle, C., Volchkov, V.E., Nichol, S.T., and Basler, C.F. (2006). Ebola virus VP24 binds karyopherin alpha1 and blocks STAT1 nuclear accumulation. J. Virol. *80*, 5156–5167.

Reid, S.P., Valmas, C., Martinez, O., Sanchez, F.M., and Basler, C.F. (2007). Ebola virus VP24 proteins inhibit the interaction of NPI-1 subfamily karyopherin alpha proteins with activated STAT1. J. Virol. *81*, 13469–13477.

Sekimoto, T., Imamoto, N., Nakajima, K., Hirano, T., and Yoneda, Y. (1997). Extracellular signal-dependent nuclear import of Stat1 is mediated by nuclear pore-targeting complex formation with NPI-1, but not Rch1. EMBO J. *16*, 7067–7077.

Tarendeau, F., Boudet, J., Guilligay, D., Mas, P.J., Bougault, C.M., Boulo, S., Baudin, F., Ruigrok, R.W., Daigle, N., Ellenberg, J., et al. (2007). Structure and nuclear import function of the C-terminal domain of influenza virus polymerase PB2 subunit. Nat. Struct. Mol. Biol. *14*, 229–233.

Valmas, C., Grosch, M.N., Schümann, M., Olejnik, J., Martinez, O., Best, S.M., Krähling, V., Basler, C.F., and Mühlberger, E. (2010). Marburg virus evades interferon responses by a mechanism distinct from ebola virus. PLoS Pathog. *6*, e1000721.

Vinkemeier, U., Cohen, S.L., Moarefi, I., Chait, B.T., Kuriyan, J., and Darnell, J.E., Jr. (1996). DNA binding of in vitro activated Stat1 alpha, Stat1 beta and truncated Stat1: interaction between NH2-terminal domains stabilizes binding of two dimers to tandem DNA sites. EMBO J. *15*, 5616–5626.

Vitalis, A., and Pappu, R.V. (2009). ABSINTH: a new continuum solvation model for simulations of polypeptides in aqueous solutions. J. Comput. Chem. *30*, 673–699.

Wälde, S., Thakar, K., Hutten, S., Spillner, C., Nath, A., Rothbauer, U., Wiemann, S., and Kehlenbach, R.H. (2012). The nucleoporin Nup358/RanBP2 promotes nuclear import in a cargo- and transport receptor-specific manner. Traffic *13*, 218–233.

Winn, M.D., Ballard, C.C., Cowtan, K.D., Dodson, E.J., Emsley, P., Evans, P.R., Keegan, R.M., Krissinel, E.B., Leslie, A.G., McCoy, A., et al. (2011). Overview of the CCP4 suite and current developments. Acta Crystallogr. D Biol. Crystallogr. *67*, 235–242.

Yarbrough, M.L., Mata, M.A., Sakthivel, R., and Fontoura, B.M. (2014). Viral subversion of nucleocytoplasmic trafficking. Traffic *15*, 127–140.

Zhang, A.P., Abelson, D.M., Bornholdt, Z.A., Liu, T., Woods, V.L., Jr., and Saphire, E.O. (2012a). The ebolavirus VP24 interferon antagonist: know your enemy. Virulence *3*, 440–445.

Zhang, A.P., Bornholdt, Z.A., Liu, T., Abelson, D.M., Lee, D.E., Li, S., Woods, V.L., Jr., and Saphire, E.O. (2012b). The ebola virus interferon antagonist VP24 directly binds STAT1 and has a novel, pyramidal fold. PLoS Pathog. *8*, e1002550.

Zhang, A.P., Bornholdt, Z.A., Abelson, D.M., and Saphire, E.O. (2014). Crystal structure of Marburg virus VP24. J. Virol. *88*, 5859–5863.